He *et al. Cancer Nano* (2019) 10:8
https://doi.org/10.1186/s12645-019-0053-0

Cancer Nanotechnology

RESEARCH Open Access

Effects and side effects of plasmonic photothermal therapy in brain tissue

Yue He, Kristoffer Laugesen, Dana Kamp, Salik A. Sultan, Lene B. Oddershede and Liselotte Jauffred*

*Correspondence:
jauffred@nbi.dk
Niels Bohr Institute, University of Copenhagen, Blegdamsvej 17, 2100 Copenhagen, Denmark

Abstract

Background: Heat generated from plasmonic nanoparticles can be utilized in plasmonic photothermal therapy. A combination of near-infrared laser and plasmonic nanoparticles is compelling for the treatment of brain cancer, due to the efficient light-to-heat conversion and bio-compatibility. However, one of the challenges of plasmonic photothermal therapy is to minimize the damage of the surrounding brain tissue. The adjacent tissue can be damaged as a result of either absorption of laser light, thermal conductivity, nanoparticles diffusing from the tumor, or a combination hereof. Hence, we still lack the full understanding of the light–tissue interaction and, in particular, the thermal response.

Results: We tested the temperature change in three different porcine cerebral tissues, i.e., the stem, the cerebrum, and the cerebellum, under laser treatment. We find that the different tissues have differential optical and thermal properties and confirm the enhancement of heating from adding plasmonic nanoparticles. Furthermore, we measure the loss of laser intensity through the different cerebral tissues and stress the importance of correct analysis of the local environment of a brain tumor.

Conclusions: Our results stress the conclusion that a personalized analysis of the local environment is needed to balance the effect and side effects prior to plasmonic photothermal therapy.

Keywords: Plasmonic nanoparticle, Photothermal therapy, Brain cancer

Background

Malignant brain tumors are either primary cancers of the central nervous system or secondary tumors arising from metastasis (Louis et al. 2016). Conventional treatments include surgery, radiotherapy, chemotherapy, and symptomatic therapies. Despite this, brain tumors are still associated with poor prognosis, for instance due to recurrence from the resection site. Due to the infiltrative growth of the tumor, any potential therapy must take care not to damage the surrounding, healthy tissue (Sedo and Mentlein 2012).

Recent advances in nanotechnology bears promise of using nanoparticles in cancer therapy as light-to-heat converters for plasmonic photothermal therapy (PPTT) (Huang et al. 2008). The therapy is based on the following principle: the electromagnetic field of a laser beam resonates with the plasmonic field of nanoparticles, which absorb the incident light (Jauffred et al. 2019). Then the absorbed energy is dissipated as heat within a distance comparable to the particle's diameter (Bendix et al. 2010). Hence, if

nanoparticles are embedded in tumors, laser irradiation will cause hyperthermia (41° –44 °C) and localized irreversible damage of the cancerous tissue (O'Neal et al. 2004). This effect is further enhanced by the fact that cancer cells are more susceptible to thermal treatment than healthy cells (van der Zee 2002). Our first choice of plasmonic nanoparticles is gold nanoshells (AuNSs) that are resonant with near-infrared (NIR) lasers (806 nm) in the the biological transparency window (Jaque et al. 2014). Furthermore, AuNSs have been shown promising for PTTP both in vitro (Qin and Bischof 2012; Pattani and Tunnell 2012) and in vivo (Huang and El-Sayed 2010; Jørgensen et al. 2016; Yang et al. 2016; Day et al. 2011; Singh et al. 2018).

There is overall two strategies of particle delivery either via inter-tumoral or intravenous injections. When injected intravenously, nanoparticles have been shown to accumulate in tumors due to the enhanced permeability and retention (EPR) effect. As this effect is size dependent, there are signs that AuNSs ($\sim$ 150 nm) accumulate less in tumors than smaller plasmonic particles ($<$ 100 nm) (Ayala-Orozco et al. 2014). Therefore, we in parallel used (70 nm) silver nanoplates (AgNP) with a resonance slightly above our NIR laser (850 nm) that have shown to heat efficiently (Marcano Olaizola 2018). One challenge, however, is the inevitable irradiation of the healthy tissue surrounding the tumor and the resulting laser-induced damage of healthy tissue. This interaction between light and tissue depends on the scattering and absorption properties of tissue as well as on the thermal conductivity and diffusivity of cerebral tissue (Jacques 2013; Yaroslavsky et al. 2002). More knowledge is needed to clarify both (i) loss of radiation in tumor tissue and (ii) unintentional heating of healthy tissue. Therefore, the work presented here provides an examination method relevant for cerebral tissue as well as tissues from other organs.

In this study, we measure the temperature change in a phantom mimicking brain tissue and also in different porcine cerebral tissues. We chose this model system because it resembles human brain more than tissues from rodents or rabbits (Howells et al. 2010). In particular, they have similar ratios of gray and white matter (Zhang and Sejnowski 2000). For all samples types investigated, we measure the temperature under laser irradiation and we find a significant difference between the heating of brain stem and the other types of tissue upon laser irradiation. In addition, we find an increased heating in tissue injected with AuNSs and AgNP upon laser irradiation, hence, hyperthermia is affirmed but the effect is diminished by the strong absorption and scattering of the brain tissue itself. Thus, we conclude that the effect of PPTT on the tumor and the side effects on the healthy brain tissue is related in a non-trivial manner, depending on the tissue properties.

Materials and methods

Artificial tissue and AuNSs and AgNP mixture preparation

The AuNSs (peak absorbance at 800 nm, NanoXact NanoComposix) have silica cores ($\sim$ 120 nm diameter) and 15-nm gold shells and polyethylene glycol coating (PEG). The AgNPs (peak absorbance at 850 nm, NanoXact NanoComposix) have an average diameter of 70 nm and a polyvinylpyrrolidone coating (PVP). The artificial tissue was made of agarose powder (A9539-50G, SIGMA) dissolved in phosphate-buffered saline (PBS) to a concentration of 0.6% (w/V) in a 100 °C water bath for 2–5 min. Once the agarose powder was dissolved, it was removed from the water bath and left to cool until the

agarose solution reached ~ 50 °C. Then the dissolved agarose was mixed with nanoparticle solution in 4.5-ml polystyrene optical cuvettes (Kartell, 634-8531) with dimensions of (1 cm) × (1 cm) × (4.5 cm). The mixed solution was left to cool and solidify on the bench. Suspensions of plasmonic nanoparticles in agarose were prepared by mixing the AuNSs or AgNPs to a final density of 5.6 μg/ml or 10–100 times diluted. The concentrations are 10–1000 times less than the concentrations used for in vivo experiments of plasmonic photothermal therapy (Jørgensen et al. 2016).

Brain sample preparation

The brain tissue was dissected from newly butchered pigs (in accordance with Danish law) and separated in 3 distinct parts: cerebrum, cerebellum, and brain stem (Fig. 1b). The fresh brain tissue was filled into the 4.5-ml cuvettes. We used a syringe to create partial vacuum in the cuvette to ease the transfer. We kept sample masses constant at (4.1 ± 0.1) g (mean ± SD) but allowed variations in volume. Before irradiation, the samples were kept at room temperature for about 2 h for calibration and we made sure that all experiments were done within the first 48 h (± 3 h).

Laser irradiation

Inspired by Ref. Cole et al. (2009) and Ref. Samadi et al. (2018) we sat up a laser irradiation and thermal imaging system based on the following components: an 806-nm laser (Modulight Inc., ML6600-0A1) transmitted through an optical fiber to an illumination kit (Modulight Inc., MLAKIT EID655369), including a lens and a horizontally placed protecting shield. We confirmed the laser power using a standard power meter (P-link; Gentec, Sweden) and measured the beam width ($1/e^2$) to be ~ 1 cm, which is the width of our cuvettes. We used an InSb IR camera (FLIR Systems SC4000, Boston, MA) with a spectral range of 3–5 μm, to measure the heating characteristics of the sample. The IR camera was mounted at a 90° angle to the laser such that the sample was irradiated completely while not interfering with the imaging. Each sample was illuminated at a constant laser power in the range from 0.5 to 2 W, which corresponds to a radiant flux per surface area, i.e., irradiance, of [0.08, 0.16, 0.24, 0.32] W/cm^2. Frame rate was 6/min. For heating–cooling cycles, we irradiated the samples for 30 min and let them cool to room temperature for another 30 min, after the laser was turned off. During the experiments, we

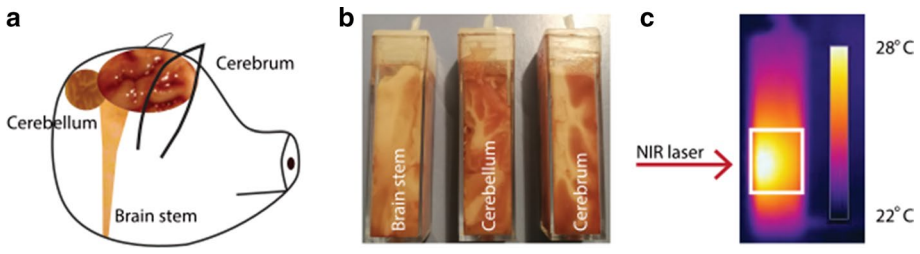

Fig. 1 Experimental setup. **a** Sketch of a pig brain's cross-section illustrating the position of the brain stem, cerebrum, and cerebellum. The structures shown here have symmetric counterparts in the other half of the brain. **b** Cuvettes with dissected cerebral tissue: Brain stem, cerebrum, and cerebellum, respectively. **c** Thermal image of a cuvette containing cerebral tissue irradiated with a NIR laser (red arrow) for 25 min. The region of interest (white box) encloses the pixels analyzed to find the maximum temperature which is denoted *T*. The color bar denotes absolute temperatures

monitored the variations in the ambient temperatures (see background in Fig. 1c) and the standard deviations of the ambient temperatures were used to filter our data using Chauvenet's criteria for data filtering.

Plasmonic photothermal heating of brain tissue

In the experiments with blended brain, we compared the brain tissues from 6 different animals. The brain samples were prepared as described above, and then blended using a centrifugal stirrer (IKA®-WERKE RW16 Basic) and a Tissue Grinder with serrated pestle (Thomas®). The homogenized brain was transferred into cuvettes with volumes of about 3.4 cm^3. We washed the nanoparticles by spinning and re-suspending in PBS. Tissue samples were injected and mixed (vortex) with 207 μl of PBS with re-suspended AuNSs or AgNPs to a density 5.8 μg/ml. The control group was injected with an equal volume of PBS.

Absorbance spectroscopy

Spectrophotometry was performed using a Cary 5000 UV–Vis–NIR spectrophotometer (Agilent). Homogenized brain tissue from cerebrum, cerebellum, and brain stem were diluted in PBS (Thermo Scientific). Dilutions of 1:2000 or 1:1000 (w/V) were used for spectrophotometry to ensure total absorbance below 1. Measurements were performed in quartz cuvettes to enable spectroscopy in the wavelength range from 350 to 1200 nm.

Data analysis

We selected a region of interest in the thermal images to obtain the maximum temperature, using the FLIR-TOOLS+ software (FLIR Sys., Boston, MA) as shown in Fig. 1c. To analyze the extracted data, we fitted the expressions given in Eqs. (1) and (2) to data. These equations were derived as detailed in Additional file 1.

Results

To measure the light-to-heat conversion, we prepared two different kinds of samples: one artificial brain phantom and one from dissected pig brain (Fig. 1a). The samples were irradiated with a NIR laser with a wavelength of 806 nm and the temperature (Fig. 1b) was recorded by an infrared (thermal) camera. Fig. 1c is an example of such a thermal image, where the temperature, T, is defined as the maximum temperature within the region of interest (white square).

Plasmonic photothermal heating of artificial tissue

We experimentally determined the heating of different concentrations of AuNSs in artificial tissue, i.e., a 0.6% agarose solution (Eldridge et al. 2016), and a control without AuNSs. Fig. 2a shows temperature change, ΔT, versus time, t, of the phantom tissue for varying particle concentration. The tissue was heated with a 1.5 W laser for half an hour and cooled (laser off) for another half an hour. The temperature driving force approximation (Bardhan et al. 2009; Roper et al. 2007; Pattani and Tunnel 2013) permits the system equilibrium time, τ, and the steady-state temperature, T_{ss}, to be estimated using

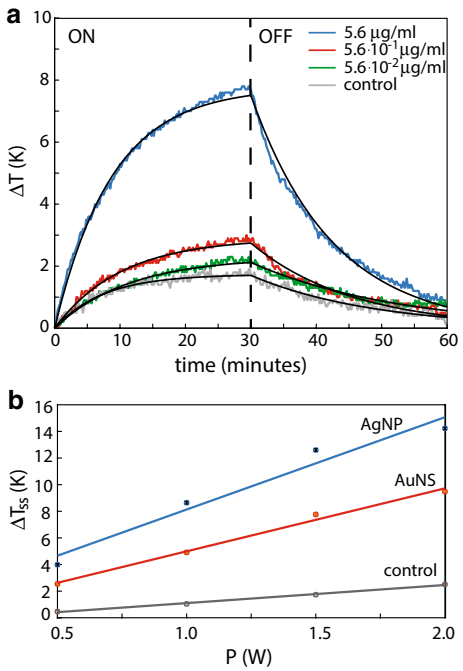

Fig. 2 Plasmonic photothermal heating of artificial tissue. **a** Temperature change, ΔT, versus time for different AuNS densities (see legends) and a control with pure agarose (light gray). The laser power, P, is 1.5 W. The 806-nm laser irradiation (ON) and without (OFF). The vertical black punctuated line signifies the instance where the laser is turned off and the full black lines are fits of Eqs. (1) and (2) to data. **b** Steady-state temperature, ΔT_{ss}, versus laser power, P, for AgNP (blue) and AuNS (red) suspensions in agarose and a control with pure agarose (gray). The particle density is 5.6 µg/ml

system parameters from heating data and cooling data, respectively. For the heating, we found the following exponential dependence on t (Roper et al. 2007):

$$\Delta T = \Delta T_{\mathrm{ss}}(1 - e^{-t/\tau}) \tag{1}$$

and for cooling:

$$\Delta T = \Delta T_{\mathrm{ss}} e^{-t/\tau}. \tag{2}$$

It is worth noticing that Eqs. (1) and (2) both are independent of the ambient temperatures. Thus, the results from this study, which were all obtained at room temperature, are also applicable at body temperature (37 °C). For the phantom tissue without AuNSs, we found $\Delta T_{\mathrm{ss}} = 1.7$ K (Fig. 2a). For a tissue at an ambient temperature of 37 °C, this corresponds to moderate hyperthermia. In contrast, we measure extreme hyperthermia ($\Delta T > 5°$ K) with 5.6 µg/ml AuNS and a laser power of 1.5 W: $\Delta T_{\mathrm{ss}} = 7.8$ K.

In a similar experiment (Fig. 2b), we kept the nanoparticle density constant at 5.6 µg/ml and varied the laser power in the range from 0.5 to 2 W. Heating rates can be deducted from the slopes of Fig. 2b and were found to be (6.9 ± 4.2) K/W for AgNP and (4.7 ± 1.3) K/W for AuNSs. Hence, in artificial tissue, the AgNPs are the most efficient nano-heaters but both nanoparticle suspension heats significantly more than the control. There is a pronounced difference in the temperature achieved and, hence, of the effect of the PTTP, depending on whether the phantom is a suspension of plasmonic nanoparticles or not. It is worth noticing that for all investigated concentrations, 50%

of ΔT_{ss} is reached within the first 7 min of irradiation. Hence, hyperthermia is reached soon after the laser is turned on.

NIR laser-induced heating of cerebrum, cerebellum, and brain stem tissue

Paralleling the experiments in phantom tissue, we investigated the temperature increase of three different types of porcine brain tissue under laser irradiation. Due to the inhomogeneous distribution of gray matter and white matter in the different samples (Fig. 1b) and in the cerebrum samples in particular, we consistently irradiated the samples from the same side to reduce the variance (cerebrum samples were irradiated from the cortex side). An example of the temperature evolution is given in Fig. 3a. The thermal reaction of the brain tissue is represented by the steady-state temperature ΔT_{ss}, which was found by fitting the heating curve of the irradiated sample with Eqs. (1) and (2). The steady-state temperature ΔT_{ss} of the three tissue types, i.e., the cerebellum, cerebrum, and brain stem, is tested for laser powers from 0.5 to 1.5 W, with 0.25 W steps and the results are shown in Fig. 3b, the error bars are weighted standard deviations of tissues

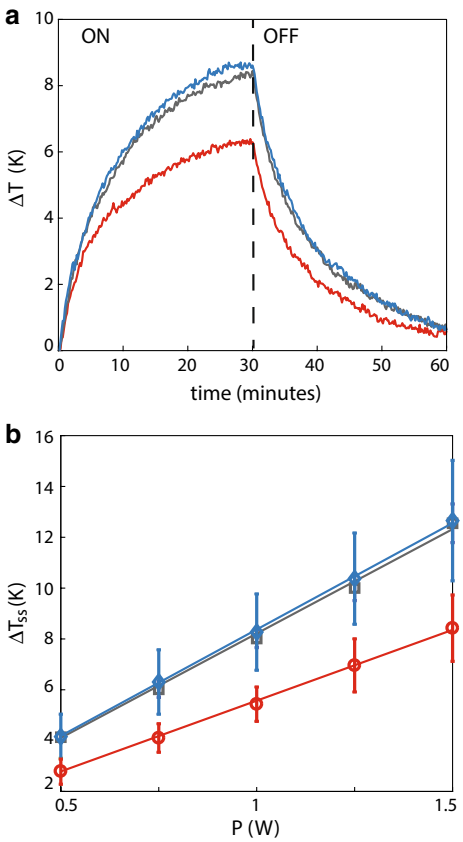

Fig. 3 NIR laser-induced heating of brain tissue. **a** ΔT versus laser power time of non-homogenized brain stem (red), cerebrum (gray), and cerebellum (blue) at a laser power, $P = 1$W. The 806-nm laser irradiation (ON) and without (OFF). The vertical black punctuated line signifies the instance where the laser is turned off. **b** Steady-state temperature ΔT_{ss} versus laser power P of non-homogenized brain stem (red circles), cerebrum (gray squares), and cerebellum (blue diamonds). The data are averaged ($N = 5$) from different animals (except for cerebellum at 0.75 W, for brain stem at 0.5 W and at 0.75 W where $N = 4$). The error bars denote one weighted standard deviations of the fitted values (Eqs. (1) and (2)) of ΔT_{ss}

from 5 different animals and the solid lines are linear fits to the data. The observed temperature increases are—like the results obtained for the artificial tissue—linearly proportional to the laser power, P. For cerebrum, cerebellum and brain stem, we found heating rates to be (8.2 ± 0.2) K/W, (8.4 ± 0.1) K/W, and (5.6 ± 0.1) K/W, respectively. Notably, the heating rate of brain stem is lower ($p << 0.05$) than the other two types of brain tissues, hence, brain stem heats significantly less when irradiated. Cerebrum and cerebellum are found to exhibit very similar heating rates ($p = 0.14$). Furthermore, the heating rates of all types of tested brain tissues are larger than for the investigated phantom tissue, which is (1.4±0.3) K/W (Fig. 2b).

Plasmonic photothermal heating of brain tissue

To investigate the heating of laser-irradiated brain tissues with plasmonic nanoparticles, we first injected AuNS into the tissue. However, it was challenging to distribute the injected particles and we did not measure any significant difference in ΔT_{ss} with or without AuNSs. Probably, this was due to the very inhomogenous distribution of the AuNSs in the tissue. To obtain a more homogeneous distribution of nanoparticles in the samples, we instead homogenized the brain tissue using a centrifugal stirrer (blender) before transferring the tissue to the cuvettes. Even though tissue homogenization disrupts the cell, membrane sheets, proteins, and ribonucleic acids remain intact (Goldberg 2014). The results of these experiments are shown in Fig. 4, which, for all three brain tissue types, displays the equilibrium temperature ΔT_{ss}, with nanoparticles (+AuNSs and +AgNP) and the control injected with the same volume of saline buffer (+PBS). Data point represents 4 or 5 independent experiments of each tissue type. Each sample is a mixture of tissue from two animals injected with either AuNS or AgNP to a final density of 5.8 μg/ml. As expected, we found that the presence of plasmonic particles significantly augment ΔT_{ss} compared to the control (+PBS) for all investigated tissue types. It is worth noticing that even though AgNPs were found to heat more efficiently than AuNSs in the artificial tissue, it is the other way around for the photothermal heating in porcine brain tissue. This is suggestive of a dramatic denaturing of the AgNP in the cerebral tissue. Therefore, an appropriate coating is needed to raise the structural stability in vivo (Espinosa et al. 2018). Still, however, for all tissue types, the effect is small compared to the experiments performed in artificial tissue where we found $\Delta T_{ss} > 4$ K (Fig. 2b). One

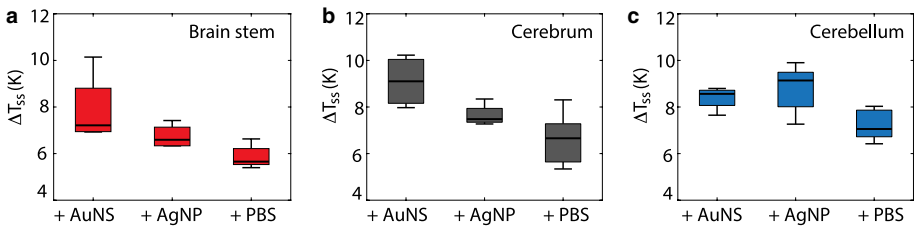

Fig. 4 Plasmonic photothermal heating of brain tissue. Box plot of the steady-state temperature, ΔT_{ss}, during laser irradiation ($P = 1$W) of homogenized cerebral tissue injected with 5.8 μg/ml AuNSs (+AuNSs) or AgNP (+AgNP). This was compared to a control injected with saline solution (+PBS). **a** Brain stem tissue with both AuNS (+AuNS, $N = 4$) and AgNP (+AgNP, $N = 4$) heats significantly more than the control (+PBS, $N = 9$) with $p = 0.003$ and $p = 0.011$, respectively. **b** Cerebrum with AuNSs (+AuNS, $p = 0.002$, $N = 4$) and AgNPs (+AgNP, $p = 0.046$, $N = 5$) and the control (+PBS, $N = 10$). **c** Cerebellum with AuNSs (+AuNS, $p = 0.004$, $N = 4$) and AgNPs (+AgNP, $p = 0.002$, $N = 5$) and the control (+PBS, $N = 10$)

obvious difference between the brain tissue and the artificial tissue, i.e., agarose, is the transparency. While the first is very dense, the artificial tissue is just slightly opaque and, hence, lets the majority of the laser light pass through the sample. To investigate this further, we measured the intensity loss in the tissue.

Absorbance spectroscopy in brain tissue

With photospectrometry in the ultraviolet to near-infrared range (UV–Vis–NIR), the absorbance of the homogenized porcine brain was evaluated. The absorbance is a dimensionless measure of the concentration-dependent attenuation or the loss of laser intensity in the tissue. To ensure accuracy, the absorbance was kept below 1 by diluting the homogenized brain tissue in a saline solution (PBS). UV–Vis–NIR spectra for the three tissue types can be seen in Fig. 5. Although the spectra have similar form, the magnitude of absorbance varies. The high absorbance of the brain stem is contradicted by the heating properties illustrated in Fig. 3, where the brain stem consistently shows a lower increase in temperature when irradiated by a laser. Since the brain stem does not absorb as much light as the other examined brain parts, scattering is suspected to be the main contributor to the measured absorbance. The curves in Fig. 5 show no signs of the absorption peaks outside of the biological window and no signs of an absorption peak when adding highly absorbent AuNSs (Additional file 2: Fig. S1). This is in agreement with the conclusion that the absorption is dwarfed by scattering.

Discussion

The effect of NIR laser radiation on biological tissue is a complex interplay between distinct phenomena: light-to-heat conversion, heat conductivity, and tissue reactions, e.g., photo-chemistry. The latter leads to denaturation—or destruction—of the tissue under treatment and depends on both laser (wavelength, power, beam profile) and on the tissue itself (optical coefficients and thermal conductivity). As the thermal conductivities of the different cerebral tissues are approximately the same

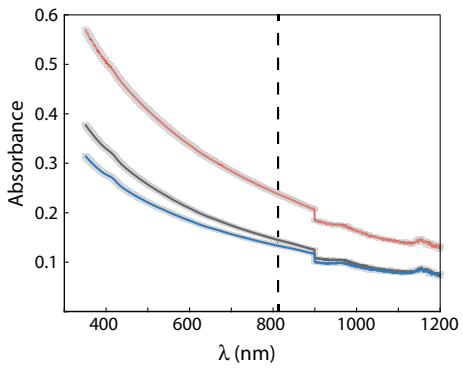

Fig. 5 UV–Vis–NIR absorbance spectra of homogenized porcine brain. Absorbance of 1:2000 times diluted tissue ($N = 3$) versus wavelength and standard deviations (light gray). Brain stem (red), cerebrum (gray), and cerebellum (blue) show similar transmittance curves, but are vertically shifted with the brain stem having the highest absorbance, followed by the cerebrum and the cerebellum, which show similar absorbances. The vertical black punctuated line signifies the wavelength (806 nm) of our laser and the jump at 900 nm is an artifact from the shift of detectors at this wavelength

(Murphy et al. 2016), we can assume the temperature rise is governed by the optical coefficients, i.e., scattering and absorption.

We found that the heating rate of brain stem (5.6 K/W) was significantly lower that the heating rates of the cerebrum (8.2 K/W) and cerebellum (8.4 K/W), which is suggestive of either lower absorption or higher scattering in brain stem tissue. This was further investigated by measurements of the attenuation (absorbance) of the laser intensity, which we found to be higher for brain stem than the other cerebral tissue types investigated. We suggest that scattering (not absorption) is dominant for brain stem tissue, which is in line with similar investigation of the optical properties of homogenized brain tissue (Eisel et al. 2018). Furthermore, these results are in correspondence with measured scattering coefficients of many different fatty tissues, see Ref. Jacques (2013) for a thorough review on the subject. Brain stem contains more white matter than cerebrum and cerebellum, which explains the more whitish color of the brain stem (Fig. 1a, b). Furthermore, it has been shown in different samples of white and gray brain matter (sliced) that white matter has substantially larger extinction coefficients than gray matter over the entire spectrum (300–1100 nm) (Yaroslavsky et al. 2002). It follows from this that our (806 nm) laser penetrates deeper into the cerebrum and the cerebellum samples than the brain stem sample. Thus, more light can be absorbed in the cerebrum and cerebellum samples than in the brain stem, which explains why the brain stem heats less (Figs. 3 and 4).

The addition of plasmonic nanoparticles to the brain tissue increases the absorption coefficient of the whole sample and causes heating. We compared the temperature rise of two different plasmonic particle suspensions of equal density in artificial tissue and found that AgNPs are better light-to-heat converters than AuNSs (Fig. 3b). Furthermore, as AgNPs are smaller than AuNS (70 nm versus 150 nm) they are prone to be up-concentrated more regularly in tumors as a consequence of the EPR effect. Unfortunately, the superior transduction efficiency was not consolidated when the AgNP were mixed with cerebral tissue (Fig. 4). We think this is a sign of AgNP's dissolving under in vivo conditions. Thus, stability—and thereby accumulation—must be further investigated to evaluate the toxicological effects of AgNPs (Zhang et al. 2018).

For the heating experiments, homogenizing the sample is beneficial in terms of comparing samples and reproducing results. In particular, for small heterogeneous samples from biopsies or resections. However, homogenization of brain tissue is reported to cause an increase in absorption and decrease in scattering coefficients, which is attributed to the more even distribution of hemoglobin and to the destruction of membranes and other cellular structures when blending the tissue (Eisel et al. 2018; Roggan et al. 1999). Furthermore, our storage of tissue may have altered the optical properties of the samples, as there are indications that refrigerating for 24–48 h can cause a decrease in absorption and an increase in scattering of homogenized porcine liver tissue. In contrast, slow freezing at −20 °C was followed by a significant decrease in both absorption and scattering coefficients (Roggan et al. 1999). In the current experiments, however, all samples were treated identically, hence, comparisons between the tissue types should be valid.

Conclusions

Given this knowledge, scattering is largely diminishing the effect of PPTT in the brain tissue. Thus, a possible implementation in the brain must take this into account and apply the laser very locally, i.e., directly in the tumor. As brain cancer often is associated with surgery, this has the potential to be combined with inter-tumoral administration of both particles and optic fibers. Due to the risk of side effects, e.g., hyperthermia and photochemistry, laser powers should be kept low to deposit a minimum of energy in healthy cerebral tissue and particle aggregation and stability should be tested. We anticipate that tissue investigations can be done in parallel with ongoing in vivo evaluation of PPTT. The potential results are twofold: (i) to measure loss of radiation in the tumor environment and (ii) to estimate the risk of damaging healthy tissue.

In conclusion, we show that the loss of radiation in tumor tissue and unintentional laser heating of the healthy tissue cannot be neglected. Thus, a personalized analysis of the local environment is needed to balance effect and side effects prior to any potential plasmonic photothermal therapy.

Supplementary information

Supplementary information accompanies this paper at https://doi.org/10.1186/s12645-019-0053-0.

Additional file 1. Derivation of heat transfer equations.

Additional file 2. UV–Vis–NIR absorbance spectra of homogenized porcine brain and AuNSs.

Abbreviations

PPTT: plasmonic photothermal therapy; EPR: enhanced permeability and retention; AuNS: gold nanoshells; AgNP: silver nanoplates.

Acknowledgements

The authors thank Harald Hansen's abattoir for providing the fresh porcine brain, Martin Roursgaard, Institute of Public Health, University of Copenhagen, for kindly providing the tissue blender, and Kamilla Nørregard for fruitful discussions.

Authors' contributions

YH, DK, and SAS did the thermal imaging assays. KL performed UV–Vis experiments. YH and LJ conceived the original idea and LJ supervised the project. LO helped supervise the project. All authors discussed the results and contributed to the final manuscript. All authors read and approved the final manuscript.

Funding

Danish National Research Councils (DNRF116) and Chinese Scholarship Council (201707940002).

Availability of data and materials

Not applicable.

Ethics approval and consent to participate

Not applicable.

Consent for publication

Not applicable.

Competing interests

The authors declare that they have no competing interests.

Received: 18 July 2019 Accepted: 4 October 2019
Published online: 24 October 2019

References

Ayala-Orozco C, Urban C, Bishnoi S, Urban A, Charron H, Mitchell T, Shea M, Nanda S, Schiff R, Halas N, Joshi A. Sub-100 nm gold nanomatryoshkas improve photo-thermal therapy efficacy in large and highly aggressive triple negative breast tumors. J Control Release. 2014;191:90–7. https://doi.org/10.1016/j.jconrel.2014.07.038. arxiv:NIHMS150003.

Bardhan R, Grady NK, Cole JR, Joshi A, Halas NJ. Fluorescence enhancement by au nanostructures: nanoshells and nanorods. ACS Nano. 2009;3(3):744–52. https://doi.org/10.1021/nn900001q.

Bendix PM, Reihani SNS, Oddershede LB. Direct measurements of heating by electromagnetically trapped gold bilayers. ACS Nano. 2010;4(4):2256–62.

Cole JR, Mirin NA, Knight MW, Goodrich GP, Halas NJ. Photothermal efficiencies of nanoshells and nanorods for clinical therapeutic applications. J Phys Chem C. 2009;113(28):12090–4. https://doi.org/10.1021/jp9003592.
Day ES, Thompson PA, Zhang L, Lewinski NA, Ahmed N, Drezek RA, Blaney SM, West JL. Nanoshell-mediated photothermal therapy improves survival in a murine glioma model. J Neuro-Oncol. 2011;104(1):55–63. https://doi.org/10.1007/s11060-010-0470-8.
Eisel M, Ströbl S, Pongratz T, Stepp H, Rühm A, Sroka R. Investigation of optical properties of dissected and homogenized biological tissue. J Biomed Opt. 2018;23(09):1. https://doi.org/10.1117/1.JBO.23.9.091418.
Eldridge BN, Bernish BW, Fahrenholtz CD, Singh R. Photothermal therapy of glioblastoma multiforme using multiwalled carbon nanotubes optimized for diffusion in extracellular space. ACS Biomater Sci Eng. 2016;2:963–76. https://doi.org/10.1021/acsbiomaterials.6b00052.
Espinosa A, Curcio A, Cabana S, Radtke G, Bugnet M, Kolosnjaj-Tabi J, Péchoux C, Alvarez-Lorenzo C, Botton GA, Silva AKA, Abou-Hassan A, Wilhelm C. Intracellular biodegradation of Ag nanoparticles, storage in ferritin, and protection by a Au shell for enhanced photothermal therapy. ACS Nano. 2018;12(7):6523–35. https://doi.org/10.1021/acsnano.8b00482.
Goldberg S. Mechanical/physical methods of cell distribution and tissue homogenization. In: Posch A, editor. 2D PAGE: sample preparation and fractionation. 1st ed. New York: Humana Press; 2014. p. 3–22. https://doi.org/10.1007/978-1-4939-2550-6.
Howells DW, Porritt MJ, Rewell SSJ, O'Collins V, Sena ES, Van Der Worp HB, Traystman RJ, MacLeod MR. Different strokes for different folks: the rich diversity of animal models of focal cerebral ischemia. J Cereb Blood Flow Metab. 2010;30(8):1412–31. https://doi.org/10.1038/jcbfm.2010.66.
Huang X, El-Sayed MA. Gold nanoparticles: optical properties and implementations in cancer diagnosis and photothermal therapy. J Adv Res. 2010;1(1):13–28. https://doi.org/10.1016/j.jare.2010.02.002.
Huang X, Jain PK, El-Sayed IH, El-Sayed MA. Plasmonic photothermal therapy (PPTT) using gold nanoparticles. Lasers Med Sci. 2008;23(3):217–28. https://doi.org/10.1007/s10103-007-0470-x.
Jacques SL. Erratum: Optical properties of biological tissues: a review (Physics in Medicine and Biology (2013) 58). Phys Med Biol. 2013;58(14):5007–8. https://doi.org/10.1088/0031-9155/58/14/5007.
Jaque D, Martínez Maestro L, Del Rosal B, Haro-Gonzalez P, Benayas A, Plaza JL, Martín Rodríguez E, García Solé J. Nanoparticles for photothermal therapies. Nanoscale. 2014;6(16):9494–530. https://doi.org/10.1039/c4nr00708e.
Jauffred L, Samadi A, Klingberg H, Bendix PM, Oddershede LB. Plasmonic heating of nanostructures. Chem Rev. 2019;. https://doi.org/10.1021/acs.chemrev.8b00738.
Jørgensen JT, Nørregaard K, Tian P, Bendix PM, Kjaer A, Oddershede LB. Single particle and PET-based platform for identifying optimal plasmonic nano-heaters for photothermal cancer therapy. Sci Rep. 2016;6(April):30076. https://doi.org/10.1038/srep30076.
Louis DN, Perry A, Reifenberger G, Deimling AV, Figarella D, Webster B, Hiroko KC, Wiestler OD, Kleihues P, Ellison DW. The 2016 World Health Organization classification of tumors of the central nervous system: a summary. Acta Neuropathol. 2016;131:803–20. https://doi.org/10.1007/s00401-016-1545-1.
Marcano Olaizola A. Photothermal determination of absorption and scattering spectra of silver nanoparticles. Appl Spectrosc. 2018;72(2):234–40. https://doi.org/10.1177/0003702817738056.
Murphy W, Black J, Hastings G. Handbook of biomaterial properties. 2nd ed. New York: Springer; 2016. https://doi.org/10.1007/978-1-4939-3305-1.
O'Neal DP, Hirsch LR, Halas NJ, Payne JD, West JL. Photo-thermal tumor ablation in mice using near infrared-absorbing nanoparticles. Cancer Lett. 2004;209(2):171–6. https://doi.org/10.1016/j.canlet.2004.02.004.
Pattani VP, Tunnell JW. Nanoparticle-mediated photothermal therapy: a comparative study of heating for different particle types. Lasers Surg Med. 2012;44(8):675–84. https://doi.org/10.1002/lsm.22072.
Pattani VP, Tunnel JW. Nanoparticle-mediated photothermal therapy: a comparative study of heating for different particle types. Lasers Surg Med. 2013;44(8):675–84. https://doi.org/10.1002/lsm.22072.Nanoparticle-mediated.
Qin Z, Bischof JC. Thermophysical and biological responses of gold nanoparticle laser heating. Chem Soc Rev. 2012;41(3):1191–217. https://doi.org/10.1039/c1cs15184c.
Roggan A, Schädel D, Netz U, Ritz J-P, Germer C-T, Müller G. The effect of preparation technique on the optical parameters of biological tissue. Appl Phys B. 1999;69:445–53. https://doi.org/10.1007/s003409900187.
Roper DK, Ahn W, Hoepfner M. Microscale heat transfer transduced by surface plasmon resonant gold nanoparticles. J Phys Chem C. 2007;111:3636–41.
Samadi A, Klingenberg H, Jauffred L, Bendix PM, Oddershede LB. Platinum nanoparticles: a non-toxic, effective and thermally stable alternative plasmonic material for cancer therapy and bioengineering. Nanoscale. 2018;10:9097.
Sedo A, Mentlein R. Glioma cell biology. Vienna: Springer; 2012. p. 1–468. https://doi.org/10.1007/978-3-7091-1431-5.
Singh P, Pandit S, Mokkapati VRSS, Garg A, Ravikumar V, Mijakovic I. Gold nanoparticles in diagnostics and therapeutics for human cancer. Int J Mol Sci. 2018;. https://doi.org/10.3390/ijms19071979.
van der Zee J. Heating the patient: a promising approach? Ann Oncol. 2002;13(8):1173–84. https://doi.org/10.1093/annonc/mdf280.
Yang T, Choi W, Yoon T, et al. In vivo photothermal treatment by the peritumoral injection of macrophages loaded with gold nanoshells. Biomed Opt Express. 2016;7(1):254667.
Yaroslavsky AN, Schulze PC, Yaroslavsky IV, Schober R, Ulrich F, Schwarzmaier HJJ. Optical properties of selected native and coagulated human brain tissues in vitro in the visible and near infrared spectral range. Phys Med Biol. 2002;47(12):2059–73. https://doi.org/10.1088/0031-9155/47/12/305.
Zhang K, Sejnowski TJ. A universal scaling law between gray matter and white matter of cerebral cortex. Proc Natl Acad Sci USA. 2000;97(10):5621–6. https://doi.org/10.1073/pnas.090504197.
Zhang W, Xiao B, Fang T. Chemical transformation of silver nanoparticles in aquatic environments: mechanism, morphology and toxicity. Chemosphere. 2018;191(7):324–34. https://doi.org/10.1016/j.chemosphere.2017.10.016.

Publisher's Note